

Numerical and Experimental Analysis of the Effects of Crack on Vibration Characteristics of GFRP-stiffened Pipes

M.H. Velayatparvardeh, A. Shooshtari*

Department of Mechanical Engineering, Faculty of Engineering, Bu-Ali Sina University, Hamedan, Iran.

Article info

Article history:

Received 28 May 2019

Received in revised form

10 September 2019

Accepted 17 September 2019

Keywords:

Composite pipe

GFRP pipe

Love theory

Vibration

Natural frequencies

Mode shapes

FRF: (Frequency Response Function)

Abstract

In this paper, the vibration characteristics of GFRP-stiffened pipes, in intact and cracked conditions are investigated. The results have different applications, which the most important ones are optimized designs of such pipes and diagnosis of the damage in them. Therefore, by Love theory, governing equations of motion for the GFRP-stiffened pipes were obtained. Having obtained characteristic equation, the natural frequencies of the problem were calculated for intact case. Then by modeling a sample of these pipes in the ANSYS software and using Modal analysis, natural frequencies and related mode shapes due to finite element method were calculated in cracked and intact conditions. Then by using the experimental modal analysis method, the natural frequencies of a sample, which was built similar to these pipes, were obtained in cracked and intact conditions. The results of the analytical method, finite element method, and the experimental modal analysis were compared and it was shown that the results have a good compatibility. The same process was performed on carbon fiber composites.

Nomenclature

u, v, z	Displacement of plate in x, y and z direction	u_0, v_0, w_0	Displacement of middle plate in x, y and z direction
G_{xy}, G_{yz}, G_{xz}	Shear deformation modules	E_{xx}, E_{yy}, E_{zz}	Elasticities modules
A_{ij}, B_{ij}, D_{ij}	Coefficients of stiffness matrix	$\sigma_\alpha, \sigma_\beta, \sigma_{\alpha\beta}$	Stresses of plate
$\bar{A}_{IJ}, \bar{B}_{IJ}, \bar{D}_{IJ}$		$\sigma_{\beta\alpha}, \sigma_{\alpha z}, \sigma_{\beta z}$	
$\hat{A}_{IJ}, \hat{B}_{IJ}, \hat{D}_{IJ}$		(α, β, z)	Coordinate axes on top of plate
$\varepsilon_{0\alpha}, \varepsilon_{0\beta}, \gamma_{0\alpha\beta}$	Strains of mid-plate	$\vartheta_{xy}, \vartheta_{yx}, \vartheta_{yz}$	Poisson ratios
$\gamma_{0\beta\alpha}, \gamma_{0\alpha z}, \gamma_{0\beta z}$		$\vartheta_{zx}, \vartheta_{yz}, \vartheta_{zy}$	
K_α, K_β	Curvatures of the plate	$\varepsilon_\alpha, \varepsilon_\beta, \gamma_{\alpha\beta}$	Strains of the plate
$K_{\alpha\beta}, K_{\beta\alpha}$		$\gamma_{\beta\alpha}, \gamma_{\alpha z}, \gamma_{\beta z}$	
$N_\alpha, N_\beta, N_{\alpha\beta}$	Internal forces of the plate	$M_\alpha, M_\beta, M_{\alpha\beta}$	Internal moments on the plate
$N_{\beta\alpha}, Q_\alpha, Q_\beta$		$M_{\beta\alpha}, P_\alpha, P_\beta$	
T	Kinetic energy of plate	q_α, q_β, q_z	Forces on cylindrical shell
I_i	Inertia momentum of plate	$\rho^{(K)}$	K_{th} layer density

*Corresponding author: A. Shooshtari (Associate Professor)

E-mail address: shooshta@basu.ac.ir

<http://dx.doi.org/10.22084/jrstan.2019.18794.1091>

ISSN: 2588-2597

φ	Angle of fiber	Ψ_α, Ψ_β	Rotation angle of plate in x, y
R_α, R_β	Radius of thick plate	W	Work of external force
z	Thickness of plate	$[\bar{Q}_{ij}]$	Stress-strain matrix
$\{F\}$	External force vector	U	Strain energy of plate
A, B	Lame's coefficients	K_i, K_j	Timoshenko stiffness coefficients
U_{mn}, V_{mn}, W_{mn}	Amplitudes of displacements and	a	Length of crack
$\Psi_{\alpha mn}, \Psi_{\beta mn}$	rotations in (m, n) mode	b	Width of crack

1. Introduction

With regard to the limits and special issues in the range of high pressure with different diameters and shortage of pipes with proper characteristics, recently a new production process for the pipe manufacturing (composite-steel) has been explored and introduced, which is the latest pipe-making technology in the world; Meanwhile, the study of dynamic and vibration behavior of composite-steel pipes is one of the most popular engineering fields. The most important step in evaluating the dynamical behavior of this type of pipes is to find the natural frequencies and the shape of the corresponding modes. Because all the dynamic behaviors of a structure are based on these two characteristics. So, in order to design and construct an optimal structure, these two features are important. One of the important issues in dynamic analysis, and in particular obtaining kinematic relations used in it, is the plate theory. Many plate theories (thin, thick, deep, shallow, etc.) reduce the three-dimensional elasticity problems into two-dimensional ones. This is possible by removing the coordinates which are perpendicular to the plate surface. The development of plate equations in the last century and the development of this kind of equations in the field of layered composite sheets have started since the midst of the 20th century. One of the studies which used the 3D elasticity theory to analyze layered plates can be found in Ye's [1] book. Bhimaraddi [2] obtained results based on the three-dimensional elasticity theory for two-curved composite shallow shells. Among other studies in this area, Wang and Lin [3], Xiaoyu [4], and Tsai [5] can be mentioned who worked on 3D elasticity theory on closed cylindrical shells. Three-dimensional solutions of cylindrical shells with initial stresses were performed by Xu et al. [6]. Ye and Soldatos [7, 8] used the 3D elasticity theory for the behavior of cylindrical shell with boundary conditions of simple-fixed support. Ding and Tang [9] performed a three-dimensional study on the free vibration of thick composite cylindrical shell with fixed-fixed boundary conditions. Chen and Shen [10], Chen et al. [11] conducted a three-dimensional study on the free vibration of isotropic cylindrical plates. Chern and Chao [12] applied the three-dimensional theory to study the natural frequencies of the curved-layered plates; however, the theory used for thick shell was different from other shell and plate theories, and was presented for the first time by Love [13] which used assumptions to analyze the bending of shells. Qatu [14] carried out studies

that included a general hypothesis that was used in many thick shell analyses. This is because the acceptable levels of additional stresses for nonlinear terms are large enough. Other extensive studies by Koiter [15], Gol'denveizer [16], Noor and Burton [17] were conducted on this subject that normal cross stresses and strains in thick shells are smaller compared to other stresses and strains. Many theories which are used in shells are gained from Love theories. A lot of these theories were expressed in the middle of the twentieth century. For example, strain and displacement relations expressed by Naghdi and Berry [18] are in contradiction with the motion of a rigid object. Since a long time ago, especially in the recent decades, various researches have been done experimentally or numerically in the field of layered composites, and in particular composite-protected pipes, which some of these articles are mentioned below: Almeida et al. [19] numerically and experimentally investigated the damage and extinction of composite pipes, reinforced with carbon/ epoxy strands under external pressure. Üstün et al. [20] investigated the effect of cracking on composite pipes, reinforced by twisted epoxy/carbon nanoparticles. Ribeiro et al. [21] conducted their research on the intersectional impact analysis on composite cylinders. Zhou et al. [22] conducted their research on the experimental and numerical analysis of transverse impact damage and the 3D transformation of circular composite pipes (circularly reinforced). Luo et al. [23] analyzed the advanced failure and energy absorption testing of composite pipes under the axial impact test. Sokolinsky et al. [24] investigated the failure of composite-reinforced pipes and the effect of the gap on structural failure. Hemmatnezhad et al. [25] performed an experimental and numerical analysis of the behavior of composite pipes of carbon- glass fibers under free vibration. Yang et al. [26] conducted their research on modal analysis on corrugated composite pipes. Gurgun and Sofuglu [27] investigated vibration characteristics of shear thickening fluid filled CFRP tubes. The vibrational properties of the structures were investigated with modal analysis, and the natural frequencies and damping ratios were calculated for two different boundary conditions (single and double-fixed ends). Capozucca and Magagnini [28] done an experimental investigation into the vibration response of homogenous beams which are strengthened by CFRP lamina and damaged by notch. The free vibration analysis of specimens were also carried out by verifying responses using numerical modelling by the Finite Ele-

ment Method (FEM). Two beam models, one with double concentrated notches and one with diffused damage, strengthened by epoxy resin in the notches and with one unidirectional CFRP lamina at the intrados were subjected to cycles of bending loading. After each cycle of static loading the free vibration response was experimentally evaluated considering the beam hinge at the ends. The envelope of Frequency Response Functions (FRFs) obtained by the dynamic experimental tests was elaborated and the changes of natural frequency values were then correlated to the damage degree both to non-strengthened beam and to the strengthened beam models also damaged by static loading. Sit and Ray [29] investigated free vibration characteristics of glass and bamboo epoxy laminates under hygrothermal effect; experimental and numerical models were developed to study the variation of vibration characteristics and other engineering properties of both types of laminates in hygrothermal environment. A finite element model based on Green-Lagrange type nonlinear third-order shear deformation theory developed to account for the nonlinear behavior induced due to hygrothermal effect.

According to the above literature survey in the opinion of the authors, there is not any research about dynamic characteristic of the steel pipes reinforced by GFRP layers. Therefore, in this research this subject was mentioned, and theoretically, numerically, and experimentally was investigated.

2. Theoretical Solution Method

2.1. The Theory of Thick Composite Sheets

The purpose of the present study is to obtain modal parameters (natural frequencies, frequency response function charts and mode shapes) of reinforced pipes with composite fiber. Due to the fact that in this problem solving, the theory of composite shells was used, first the composite sheet should be specified as a thick or a thin plate. Fig. 1 shows a sample of steel pipe reinforced by three-layer composite fiber and its cross-section area.



The mentioned GFRP pipe specifications table is as the following:

Table 1
Geometrical parameters of the present GFRP shell model.

Layer 1: Steel St-37	
Inner radius (mm)	23.75
Outter radius (mm)	25
Layer thickness (mm)	1.25
Length of shell (mm)	300
Layer 2: E-Glass/Epoxy	
Inner radius (mm)	25
Outter radius (mm)	25.5
Layer thickness (mm)	0.5
Length of shell (mm)	300
Composite fiber angle (θ°)	30
Layer 3: E-Glass/Epoxy	
Inner radius (mm)	25.5
Outter radius (mm)	26
Layer thickness (mm)	0.5
Length of shell (mm)	300
Composite fiber angle (θ°)	-30

Additionally, the mechanical specifications of the used material in GFRP pipe layers are in Table 2.

Table 2
Material properties of the present GFRP shell model.

Layer 1: Steel St-37		
Young's modulus (GPa)	E	210
Shear modulus (GPa)	G	81
Poisson's ratio	ν	0.3
Density (kg/m^3)	ρ	7850
Layer 2, 3: E- Glass/ Epoxy		
Young's Modulus (Gpa)	$E_{11},$ $E_{22},$ E_{33}	45, 10, 10
Shear Modulus (Gpa)	$G_{12},$ $G_{23},$ G_{31}	5, 3.8462, 5
Poisson's ratio	$\nu_{12},$ $\nu_{23},$ ν_{31}	0.3, 0.4, 0.3
Density (kg/m^3)	ρ	2000

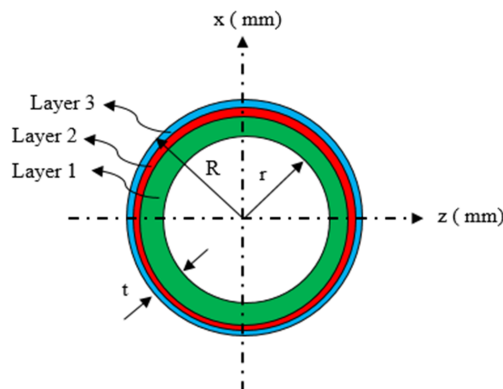


Fig. 1. A view of the GFRP pipe and its cross-sectional area.

Using the specifications stated in the Fig. 1 and also Tables 1 and 2 and based on Love theory of thick shells, the free vibrational solution and problem was done to obtain the modal parameters of the GFRP pipe. A composite cylindrical sheet which is located on the coordinate system (α, β, n) is shown in the Fig. 2.

The strain-displacement relations are:

$$\begin{aligned} \varepsilon_{0\alpha} &= \frac{\partial u_0}{\partial \alpha}, \quad \varepsilon_{0\beta} = \frac{\partial v_0}{\partial \beta} + \frac{w_0}{R}, \quad \varepsilon_{0\alpha\beta} = \frac{\partial v_0}{\partial \alpha}, \quad \varepsilon_{0\beta\alpha} = \frac{\partial u_0}{\partial \beta} \\ \gamma_{0\alpha z} &= \frac{\partial w_0}{\partial \alpha} + \Psi_\alpha, \quad \gamma_{0\beta z} = \frac{\partial w_0}{\partial \beta} - \frac{v_0}{R} + \Psi_\beta, \quad K_\alpha = \frac{\partial \Psi_\alpha}{\partial \alpha}, \\ K_\beta &= \frac{\partial \Psi_\beta}{\partial \beta}, \quad K_{\alpha\beta} = \frac{\partial \Psi_\beta}{\partial \alpha}, \quad K_{\beta\alpha} = \frac{\partial \Psi_\alpha}{\partial \beta} \end{aligned} \quad (1)$$

In the above relations, u_0 , v_0 , and w_0 are the displacements of the middle plane which is introduce as:

$$u_0(\alpha, \beta, t) = \sum_{m=0}^M \sum_{n=0}^N U_{mn} \cos(\alpha_m \alpha) \sin(n\theta) \sin(\omega_{mn} t)$$

$$v_0(\alpha, \beta, t) = \sum_{m=0}^M \sum_{n=0}^N V_{mn} \sin(\alpha_m \alpha) \cos(n\theta) \sin(\omega_{mn} t)$$

$$\begin{aligned} w_0(\alpha, \beta, t) &= \sum_{m=0}^M \sum_{n=0}^N W_{mn} \sin(\alpha_m \alpha) \sin(n\theta) \sin(\omega_{mn} t) \\ \alpha_m &= \frac{m\pi}{a}, \quad \omega_{mn} = \text{Natural frequency} \end{aligned} \quad (2)$$

The stress-force relations of the cylindrical shell are:

$$\begin{aligned} \begin{bmatrix} N_\alpha \\ N_{\alpha\beta} \\ Q_\alpha \end{bmatrix} &= \int_{-\frac{h}{2}}^{\frac{h}{2}} \begin{bmatrix} \sigma_\alpha \\ \sigma_{\alpha\beta} \\ \sigma_{\alpha z} \end{bmatrix} \left(1 + \frac{z}{R}\right) dz, \\ \begin{bmatrix} N_\beta \\ N_{\beta\alpha} \\ Q_\beta \end{bmatrix} &= \int_{-\frac{h}{2}}^{\frac{h}{2}} \begin{bmatrix} \sigma_\beta \\ \sigma_{\beta\alpha} \\ \sigma_{\beta z} \end{bmatrix} \left(1 + \frac{z}{R}\right) dz, \\ \begin{bmatrix} M_\alpha \\ M_{\alpha\beta} \\ P_\alpha \end{bmatrix} &= \int_{-\frac{h}{2}}^{\frac{h}{2}} \begin{bmatrix} \sigma_\alpha \\ \sigma_{\alpha\beta} \\ \sigma_{\alpha z} \end{bmatrix} \left(1 + \frac{z}{R}\right) z dz \\ \begin{bmatrix} M_\beta \\ M_{\beta\alpha} \\ P_\beta \end{bmatrix} &= \int_{-\frac{h}{2}}^{\frac{h}{2}} \begin{bmatrix} \sigma_\beta \\ \sigma_{\beta\alpha} \\ \sigma_{\beta z} \end{bmatrix} \left(1 + \frac{z}{R}\right) z dz \end{aligned} \quad (3)$$

To calculate the moments and forces expressed in Eq. (3), the following relationships are used:

$$\begin{aligned} \begin{bmatrix} N_\alpha \\ N_\beta \\ N_{\alpha\beta} \\ N_{\beta\alpha} \\ M_\alpha \\ M_\beta \\ M_{\alpha\beta} \\ M_{\beta\alpha} \end{bmatrix} &= \begin{bmatrix} \bar{A}_{11} & A_{12} & \bar{A}_{16} & A_{16} & \bar{B}_{11} & B_{12} & \bar{B}_{16} & B_{16} \\ A_{12} & \hat{A}_{22} & A_{26} & \hat{A}_{26} & B_{12} & \hat{B}_{22} & \bar{B}_{26} & \hat{B}_{26} \\ \bar{A}_{16} & A_{26} & \bar{A}_{66} & A_{66} & \bar{B}_{16} & B_{26} & \bar{B}_{66} & \hat{B}_{66} \\ A_{16} & \hat{A}_{26} & A_{66} & \hat{A}_{66} & B_{16} & \hat{B}_{26} & \bar{B}_{66} & \hat{B}_{66} \\ \bar{B}_{11} & B_{12} & \bar{B}_{16} & B_{16} & \bar{D}_{11} & D_{12} & \bar{D}_{16} & D_{16} \\ B_{12} & \hat{B}_{22} & B_{26} & \hat{B}_{26} & D_{12} & \hat{D}_{22} & D_{26} & \hat{D}_{26} \\ \bar{B}_{16} & B_{26} & \bar{B}_{66} & B_{166} & \bar{D}_{16} & D_{26} & D_{66} & D_{66} \\ B_{16} & \hat{B}_{26} & B_{66} & \hat{B}_{66} & D_{16} & \hat{D}_{26} & D_{66} & \hat{D}_{66} \end{bmatrix} \begin{bmatrix} \varepsilon_{0\alpha} \\ \varepsilon_{0\beta} \\ \varepsilon_{0\alpha\beta} \\ \varepsilon_{0\beta\alpha} \\ K_\alpha \\ K_\beta \\ K_{\alpha\beta} \\ K_{\beta\alpha} \end{bmatrix} \\ \begin{bmatrix} Q_\alpha \\ Q_\beta \\ P_\alpha \end{bmatrix} &= \begin{bmatrix} \bar{A}_{55} & A_{45} & \bar{B}_{55} \\ A_{45} & \hat{A}_{44} & B_{45} \\ \bar{B}_{55} & B_{45} & \bar{D}_{55} \end{bmatrix} \begin{bmatrix} \gamma_{0\alpha z} \\ \gamma_{0\beta z} \\ \frac{\Psi_\alpha}{R} \end{bmatrix} \end{aligned} \quad (4)$$

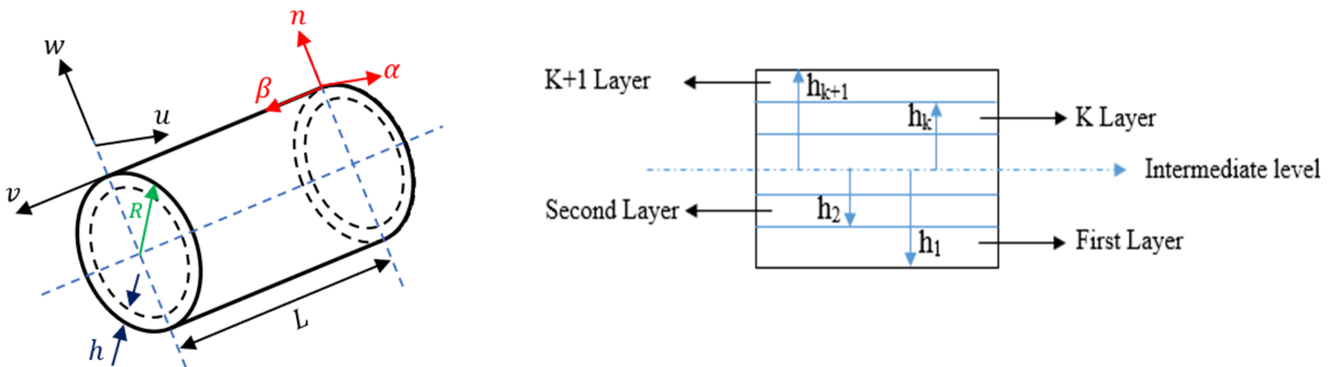


Fig. 2. A view of composite cylindrical shell and its cross-section.

In Eq. (4), N_α , N_β , Q_α , and Q_β , are the vertical forces in the main directions α and β . Also, $N_{\alpha\beta}$ and $N_{\beta\alpha}$ are the shear forces on the center plane, in the footnote of which they are intended for the first footprint perpendicular to the desired force and second footer for tangent force. M_α , M_β , $M_{\alpha\beta}$, $M_{\beta\alpha}$, P_α and P_β are all the moments on the middle plane of the cylindrical shell. Also, the coefficients A , B , and D are introduced as:

$$\begin{cases} A_{ij} = \sum_{K=1}^N \bar{Q}_{ij}^{(K)} (h_k - h_{k-1}) \\ B_{ij} = \frac{1}{2} \sum_{K=1}^N \bar{Q}_{ij}^{(K)} (h_k^2 - h_{k-1}^2) : i, j = 1, 2, 6 \\ D_{ij} = \frac{1}{3} \sum_{K=1}^N \bar{Q}_{ij}^{(K)} (h_k^3 - h_{k-1}^3) \end{cases}$$

$$\begin{cases} A_{ij} = \sum_{K=1}^N K_i K_j \bar{Q}_{ij}^{(K)} (h_k - h_{k-1}) \\ B_{ij} = \frac{1}{2} \sum_{K=1}^N K_i K_j \bar{Q}_{ij}^{(K)} (h_k^2 - h_{k-1}^2) : i, j = 4, 5 \\ D_{ij} = \frac{1}{3} \sum_{K=1}^N K_i K_j \bar{Q}_{ij}^{(K)} (h_k^3 - h_{k-1}^3) \end{cases} \quad (5)$$

$$\begin{cases} \bar{A}_{IJ} = A_{ij} + \frac{B_{ij}}{R}, \hat{A}_{IJ} = A_{ij} - \frac{B_{ij}}{R} \\ \bar{B}_{IJ} = B_{ij} + \frac{D_{ij}}{R}, \hat{B}_{IJ} = B_{ij} - \frac{D_{ij}}{R} : i, j = 1, 2, 3, 4, 5, 6 \\ \bar{D}_{IJ} = D_{ij} + \frac{E_{ij}}{R}, \hat{D}_{IJ} = D_{ij} - \frac{E_{ij}}{R} \end{cases}$$

Also K_i and K_j are the coefficients of shear forces:

$$K_i = K_j = \frac{4}{5} \quad (6)$$

Fig. 3, shows the cross-section of the GFRP-stiffened pipe.

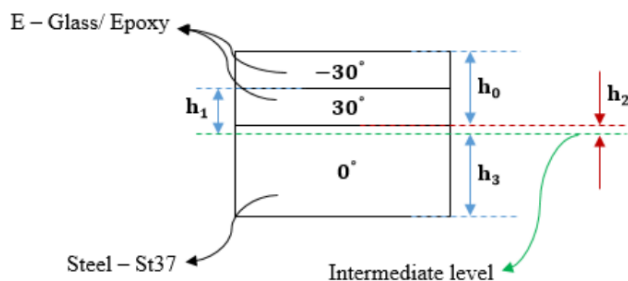


Fig. 3. The element cross section of the GFRP pipe.

Fig. 3, shows the cross-section of the GFRP-stiffened pipe. According to Fig. 3, the coefficients for $\bar{Q}_{ij}^{(K)}$ are extracted from the following formulas:

$$\begin{aligned} \bar{Q}_{11} = & Q_{11} \cos^4 \theta + 2(Q_{12} + Q_{26}) \cos^2 \theta \sin^2 \theta \\ & + Q_{22} \sin^4 \theta \end{aligned}$$

$$\begin{aligned} \bar{Q}_{12} = & (Q_{11} + Q_{22} - 4Q_{66}) \cos^2 \theta \sin^2 \theta \\ & + Q_{12} (\cos^4 \theta + \sin^4 \theta) \\ \bar{Q}_{13} = & Q_{13} \cos^2 \theta + Q_{23} \sin^2 \theta \\ \bar{Q}_{16} = & -Q_{22} \cos \theta \sin^3 \theta + Q_{11} \sin \theta \cos^3 \theta \\ & - (Q_{12} + 2Q_{66}) (\cos \theta \sin \theta) (\cos^2 \theta - \sin^2 \theta) \\ \bar{Q}_{23} = & Q_{23} \cos^2 \theta + Q_{13} \sin^2 \theta, \quad \bar{Q}_{33} = Q_{33} \\ \bar{Q}_{26} = & Q_{11} \cos \theta \sin^3 \theta - Q_{22} \sin \theta \cos^3 \theta \\ & - (Q_{12} + 2Q_{66}) (\cos \theta \sin \theta) (\cos^2 \theta - \sin^2 \theta) \\ \bar{Q}_{36} = & (Q_{13} - Q_{22}) \cos \theta \sin \theta \\ \bar{Q}_{66} = & (Q_{11} + A_{22} - 2Q_{12}) \cos^2 \theta \sin^2 \theta \\ & + Q_{66} (\cos^2 \theta - \sin^2 \theta)^2 \\ \bar{Q}_{44} = & Q_{44} \cos^2 \theta + Q_{55} \sin^2 \theta \\ \bar{Q}_{55} = & Q_{55} \cos^2 \theta + Q_{44} \sin^2 \theta \\ \bar{Q}_{45} = & (Q_{55} - Q_{44}) \cos \theta \sin \theta \end{aligned} \quad (7)$$

According to Table 2, the coefficients of Q_{ij} are obtained using the following formulas:

$$Q_{11} = E_{11} \frac{1 - \vartheta_{23}\vartheta_{32}}{\Delta}, \quad Q_{22} = E_{22} \frac{1 - \vartheta_{13}\vartheta_{31}}{\Delta}$$

$$Q_{33} = E_{33} \frac{1 - \vartheta_{12}\vartheta_{21}}{\Delta}, \quad Q_{44} = G_{23},$$

$$Q_{55} = G_{13}, \quad Q_{66} = G_{12},$$

$$Q_{12} = E_{11} \frac{\vartheta_{21} + \vartheta_{31}\vartheta_{23}}{\Delta} = E_{22} \frac{\vartheta_{12} + \vartheta_{32}\vartheta_{13}}{\Delta} \quad (8)$$

$$Q_{13} = E_{11} \frac{\vartheta_{31} + \vartheta_{21}\vartheta_{32}}{\Delta} = E_{22} \frac{\vartheta_{13} + \vartheta_{12}\vartheta_{23}}{\Delta}$$

$$Q_{23} = E_{11} \frac{\vartheta_{32} + \vartheta_{12}\vartheta_{31}}{\Delta} = E_{22} \frac{\vartheta_{23} + \vartheta_{21}\vartheta_{13}}{\Delta}$$

$$\Delta = 1 - \vartheta_{12}\vartheta_{21} - \vartheta_{23}\vartheta_{32} - \vartheta_{31}\vartheta_{13} - 2\vartheta_{21}\vartheta_{32}\vartheta_{13}$$

Substituting Eqs. (1) and (5) in the Eq. (4), the forces and moments of the cylindrical thick shell are obtained. Then, replacing the stresses obtained from Eq. (4) in Eq. (3), the stresses on the sheet can be obtained. In order to obtain the equations of motion, the Hamilton principle which is describe as follow, is used:

$$\delta \int_{t_1}^{t_2} (T - U + W) dt = 0 \quad (9)$$

In Eq. (9), T is kinetic energy, U is potential energy, and W is external work. Using the following relations:

$$\begin{aligned}
 T &= \frac{1}{2} \int_V \{\dot{u}^2 + \dot{v}^2 + \dot{w}^2\} dV \\
 &= \frac{1}{2} \int_{\alpha} \int_{\beta} \int_{-\frac{h}{2}}^{\frac{h}{2}} \{\dot{u}_0^2 + \dot{v}_0^2 + \dot{w}_0^2 + z^2(\dot{\Psi}_{\alpha}^2 + \dot{\Psi}_{\beta}^2 + 2\dot{u}_0\dot{\Psi}_{\alpha} \\
 &\quad + 2\dot{v}_0\dot{\Psi}_{\beta})\} \left\{1 + \frac{z}{R_{\alpha}}\right\} \left\{1 + \frac{z}{R_{\beta}}\right\} AB d\alpha d\beta dz \\
 U &= \frac{1}{2} \int_{\alpha} \int_{\beta} \{N_{\alpha}\varepsilon_{0\alpha} + N_{\beta}\varepsilon_{0\beta} + N_{\alpha\beta}\varepsilon_{0\alpha\beta} + N_{\beta\alpha}\varepsilon_{0\beta\alpha} \\
 &\quad + M_{\alpha}K_{\alpha} + M_{\beta}K_{\beta} + M_{\alpha\beta}K_{\alpha\beta} + M_{\beta\alpha}K_{\beta\alpha} + Q_{\alpha}\gamma_{0\alpha z} \\
 &\quad + Q_{\beta\alpha}\gamma_{0\beta\alpha} + P_{\alpha}\frac{\Psi_{\alpha}}{R_{\alpha}} + P_{\beta}\frac{\Psi_{\beta}}{R_{\beta}}\} AB d\alpha d\beta \\
 W &= \int_{\alpha} \int_{\beta} \{q_{\alpha}u_0 + q_{\beta}v_0 + q_z w_0 + m_{\alpha}\Psi_{\alpha} \\
 &\quad + m_{\beta}\Psi_{\beta}\} AB d\alpha d\beta \\
 [I_1, I_2, I_3, I_4, I_5] &= \sum_{K=1}^N \int_{h_{K-1}}^{h_K} \rho^{(K)} [1, z, z^2, z^3, z^4] dz
 \end{aligned} \tag{10}$$

and substituting the Eq. (10) in Eq. (9), the equations of motion for the cylindrical thick shell are obtained as:

$$\begin{aligned}
 \frac{\partial N_{\alpha}}{\partial \alpha} + \frac{\partial N_{\beta\alpha}}{\partial \beta} + q_{\alpha} &= (\bar{I}_1 \ddot{u}_0^2 + \bar{I}_2 \ddot{\Psi}_{\alpha}^2) \\
 \frac{\partial N_{\beta}}{\partial \beta} + \frac{\partial N_{\alpha\beta}}{\partial \alpha} + q_{\beta} &= (\bar{I}_1 \ddot{v}_0^2 + \bar{I}_2 \ddot{\Psi}_{\beta}^2) \\
 -\frac{\partial N_{\beta}}{R} + \frac{\partial Q_{\alpha}}{\partial \alpha} + \frac{\partial Q_{\beta}}{\partial \beta} + q_z &= (\bar{I}_1 \ddot{w}_0^2) \\
 \frac{\partial M_{\alpha}}{\partial \alpha} + \frac{\partial M_{\alpha\beta}}{\partial \beta} - Q_{\alpha} + m_{\alpha} &= (\bar{I}_2 \ddot{u}_0^2 + \bar{I}_3 \ddot{\Psi}_{\alpha}^2) \\
 \frac{\partial M_{\beta}}{\partial \beta} + \frac{\partial M_{\alpha\beta}}{\partial \alpha} - Q_{\beta} + m_{\beta} &= (\bar{I}_2 \ddot{v}_0^2 + \bar{I}_3 \ddot{\Psi}_{\beta}^2)
 \end{aligned} \tag{11}$$

where

$$\begin{aligned}
 u_0(\alpha, \beta, z) &= \sum_{m=1}^{\infty} \sum_{n=1}^{\infty} U_{mn} \cos(\alpha_m \alpha) \sin(\beta_n \beta) \sin(\omega_{mn} z) \\
 v_0(\alpha, \beta, z) &= \sum_{m=1}^{\infty} \sum_{n=1}^{\infty} V_{mn} \sin(\alpha_m \alpha) \cos(\beta_n \beta) \sin(\omega_{mn} z) \\
 w_0(\alpha, \beta, z) &= \sum_{m=1}^{\infty} \sum_{n=1}^{\infty} W_{mn} \sin(\alpha_m \alpha) \sin(\beta_n \beta) \sin(\omega_{mn} z) \\
 \Psi_{\alpha}(\alpha, \beta, z) &= \sum_{m=1}^{\infty} \sum_{n=1}^{\infty} \Psi_{\alpha mn} \cos(\alpha_m \alpha) \sin(\beta_n \beta) \sin(\omega_{mn} z)
 \end{aligned}$$

$$\begin{aligned}
 \Psi_{\beta}(\alpha, \beta, z) &= \sum_{m=1}^{\infty} \sum_{n=1}^{\infty} \Psi_{\beta mn} \sin(\alpha_m \alpha) \cos(\beta_n \beta) \sin(\omega_{mn} z) \\
 \alpha_m = \frac{m\pi}{R} (m = 1, 2, \dots), \quad \beta_n = \frac{n\pi}{L} (n = 0, 1, 2, \dots)
 \end{aligned} \tag{12}$$

By inserting the Eq. (12) inside (11) and using the discrete Fourier transform, the vibrating equation of the cylinder of a thick wall is obtained as follows:

$$[K] + (\omega_{mn})^2 [M] = 0 \tag{13}$$

In Eq. (13), $[K]$ is stiffness matrix and $[M]$ is mass matrix, which are defined as:

$$\begin{aligned}
 [K] &= \begin{bmatrix} K_{11} & K_{12} & K_{13} & K_{14} & K_{15} \\ K_{12} & K_{22} & K_{23} & K_{24} & K_{25} \\ K_{13} & K_{23} & K_{33} & K_{34} & K_{35} \\ K_{14} & K_{24} & K_{34} & K_{44} & K_{45} \\ K_{15} & K_{25} & K_{35} & K_{45} & K_{55} \end{bmatrix} \\
 [M] &= \begin{bmatrix} M_{11} & M_{12} & M_{13} & M_{14} & M_{15} \\ M_{12} & M_{22} & M_{23} & M_{24} & M_{25} \\ M_{13} & M_{23} & M_{33} & M_{34} & M_{35} \\ M_{14} & M_{24} & M_{34} & M_{44} & M_{45} \\ M_{15} & M_{25} & M_{35} & M_{45} & M_{55} \end{bmatrix}
 \end{aligned} \tag{14}$$

The coefficients of the above matrices are obtained as follows:

$$\begin{aligned}
 K_{11} &= -\bar{A}_{11}\alpha_m^2 - \hat{A}_{66}\beta_n^2 \\
 K_{12} &= -(A_{12} + A_{66})\alpha_m\beta_n \\
 K_{13} &= \left[\frac{A_{12}}{R}\right]\alpha_m \\
 K_{14} &= -\bar{B}_{11}\alpha_m^2 - \hat{B}_{66}\beta_n^2 \\
 K_{15} &= -(B_{12} + B_{66})\alpha_m\beta_n \\
 K_{22} &= -\bar{A}_{66}\alpha_m^2 - \hat{A}_{22}\beta_n^2 - \frac{\hat{A}_{44}}{R} \\
 K_{23} &= \left[\frac{\hat{A}_{22} + \hat{A}_{44}}{R}\right]\beta_n \\
 K_{24} &= -(B_{12} + B_{66})\alpha_m\beta_n \\
 K_{25} &= -\bar{B}_{66}\alpha_m^2 + B_{22}\beta_n^2 + \frac{\hat{A}_{44}}{R} \\
 K_{33} &= -\bar{A}_{55}\alpha_m^2 - \hat{A}_{44}\beta_n^2 - \frac{\hat{A}_{22}}{R} \\
 K_{34} &= \left[-\bar{A}_{55} + \frac{B_{12}}{R}\right]\alpha_m \\
 K_{44} &= -\bar{A}_{55} - \bar{D}_{11}\alpha_m^2 - \hat{D}_{66}\beta_n^2 \\
 K_{45} &= -(D_{12} + D_{66})\alpha_m\beta_n
 \end{aligned} \tag{15}$$

$$K_{55} = -\hat{A}_{44} - \hat{D}_{66}\alpha_m^2 - \hat{D}_{22}\beta_n^2$$

$$M_{11} = M_{22} = M_{33} = -\left(I_1 + \frac{I_2}{R}\right)$$

$$M_{14} = M_{25} = -\left(I_2 + \frac{I_3}{R}\right)$$

$$M_{44} = M_{55} = -\left(I_3 + \frac{I_4}{R}\right)$$

By placing the Eq. (15) in (13) and calculating the following determinant, the natural frequencies of the structure are obtained.

$$|[K] + (\omega_{mn})^2[M]| = 0 \quad (16)$$

The free-free boundary conditions for the problem are considered which is describe as:

$$\begin{aligned} \text{at } : x = 0 : Q_x = M_x = u_0 = v_0 = 0 \\ \text{at } : x = L : Q_x = M_x = u_0 = N_{xy} = 0 \end{aligned} \quad (17)$$

To obtain non-dimensional natural frequencies, the following formula is used:

$$\Omega = \omega_{mn}R\sqrt{\frac{\rho(1-\nu^2)}{E}} \quad (18)$$

In Eq. (18), Ω is the non-dimensional frequency, ω_{mn} is the complex natural frequency, R is the radius, ρ is the density, ν is the Poisson's ratio and E is the modulus of elasticity associated with the cylindrical shell.

For investigating the crack effects in the mathematical modelling, the crack was considered as an open crack. For this purpose, local flexibility coefficients were added to the model, based on the work of Yu et. al. [30]. In this model, the proposed equations consider the influence of the crack orientation on the local flexibility coefficient. An adaptive Simpson method was used to calculate the local flexibility coefficients of a cracked pipe.

The development of the crack in composites reinforced with brittle fibers is generally accompanied with the rupture of single fibers, the exfoliation of broken filaments of the matrix, the collapse of surrounding filaments due to localized overloading, etc. The study of the dynamic effects, related with the stress distribution during rupture of fibers and their separation of the matrix, gives new aspects about the interrelation of these micro-mechanisms of fracture and allows the development of algorithms that make computer simulation possible.

3. Finite Element Analysis (FEA)

3.1. Simulation of GFRP Pipe

The modeling of an intact GFRP pipe with geometrical and mechanical properties which are described in

Table 1 and 2 was done using ANSYS 18 software; this model is shown in Fig. 4. The member of elements were increased to 178502 to reach a convergence in the results. The GFRP pipe was meshed with Quadrilateral Dominant (Quad/Tri).

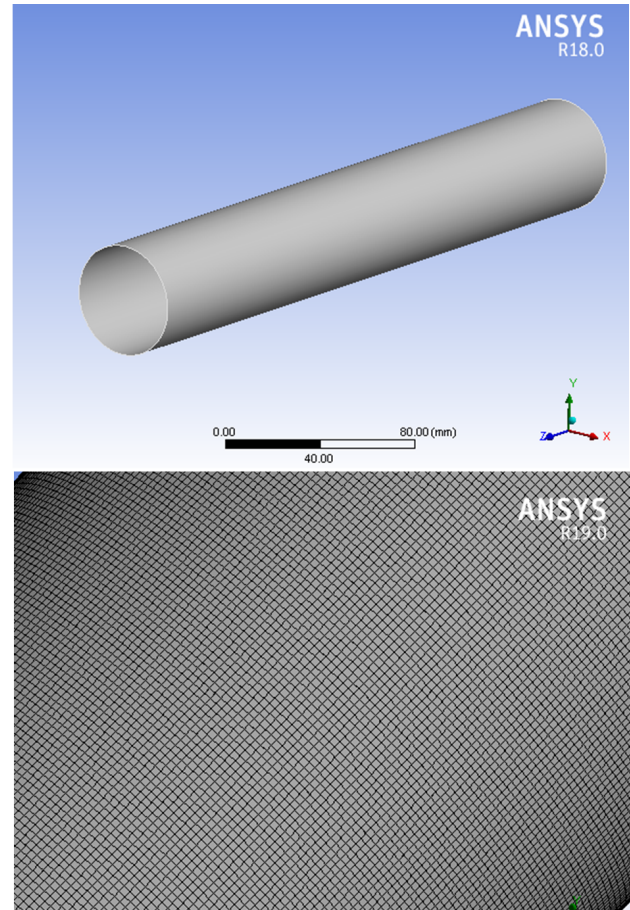


Fig. 4. Simulating a healthy and meshed GFRP pipe.

Fig. 5, shows the simulation of GFRP layers. According to this figure, one can see the orientation and angle of fibers in two layers which are selected as $+30^\circ$ and -30° .

3.2. Simulation of Cracked GFRP Pipe

In this section, a crack created on the GFRP pipe model. The location of created crack is in the middle length of pipe. Also, the parameters of the crack including length (a) and width (b) were selected based on the analytical model [30] and are shown in Fig. 6. Moreover, the depth of crack considered equal to the thickness of pipe. Therefore, the crack was as part-through type. Based on Figs. 6 and 7, the crack characteristics are as follows:

1. It is transverse and has an elliptical shape.
2. The crack position is in the middle of the pipe, 150(mm).

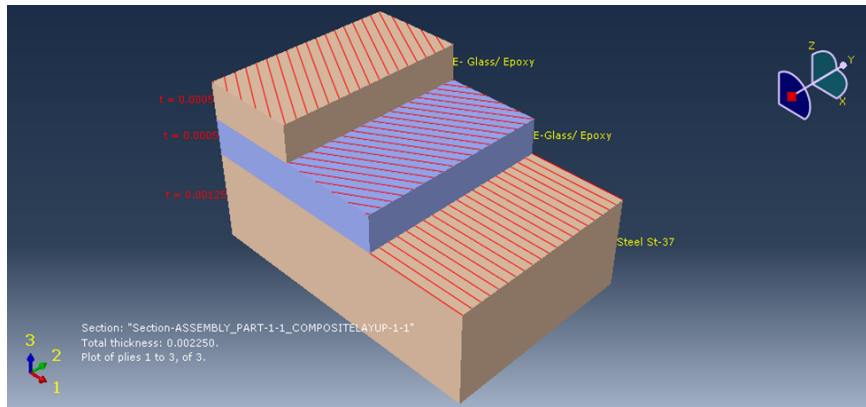


Fig. 5. A view of the GFRP pipe layers with a $30^\circ / -30^\circ$ composite fiber angle.

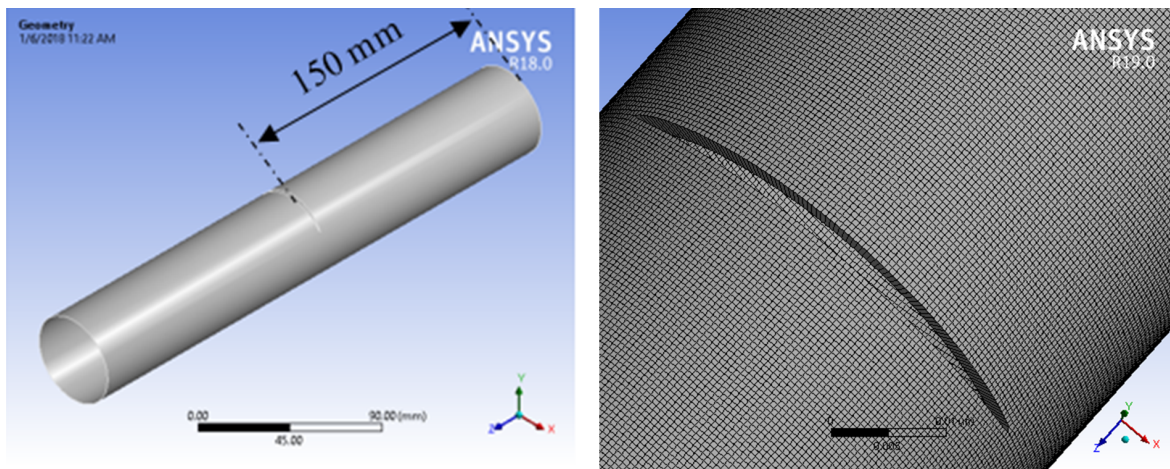


Fig. 6. Simulating a cracked and meshed GFRP pipe.

3. The bigger diameter of the oval: crack length: $(2a) = 41(\text{mm}) = \frac{1}{4}$ circumference of the pipe.
4. The smaller diameter of the oval: crack width: $(2b) = 2(\text{mm})$

4. Experimental Modal Analysis (EMA)

Modal analysis done in laboratory conditions for two models of intact and cracked GFRP pipes separately.

To perform a modal test, first the manufactured GFRP pipe has been meshed as shown in Fig. 1. The number of available meshed elements 50 and the number of nodes were 55.

4.1. Modal Analysis of Healthy GFRP Pipes

According to Fig. 8, the healthy GFRP bounded in the laboratory and the modal test done and the results were subsequently obtained. The pipe hung from the fixture with two ropes and so Free-Free-boundary condition was satisfied.

Using a modal hammer and a modal accelerometer, which was connected to pipe, modal testing was done using hammer routing method.

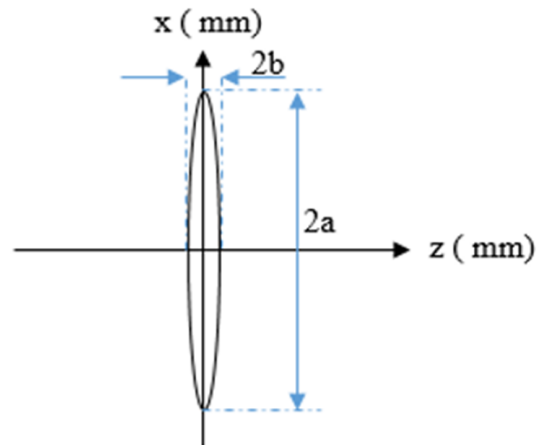


Fig. 7. Coordinate and dimensional of crack.

4.2. Modal Analysis of Cracked GFRP Pipe

As stated in Section 3.2, a crack was created using wire cut machine tool on the GFRP pipe with specific dimensions and specifications. Then, modal testing experiment was done on the specimen again under the same conditions which is shown in Fig. 9. Based on the above explanation, the created crack was a notch and not an imperfection.

5. Results and Discussion

The goal of this study is to analyze GFRP pipes in both cracked and intact conditions by theoretical method, software simulation, and laboratory modal ex-

periments and obtaining the modal characteristics of the pipe. (natural frequencies, modal shape and frequency response function). The results of the simulations are shown in Table 3.

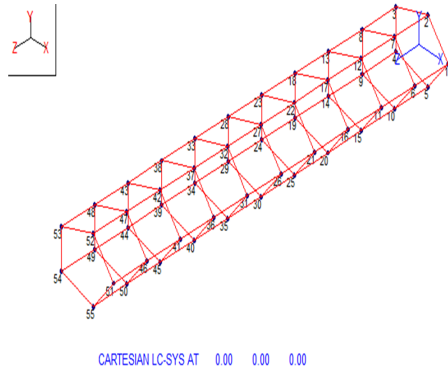


Fig. 8. Experimental modal analysis of healthy GFRP pipes.

Table 3
Natural frequencies and mode shapes for a Free-Free healthy and cracked GFRP.

Mode	FEA healthy GFRP mode (m, n)	FEA Cracked GFRP mode (m, n)	Mode	FEA healthy GFRP mode (m, n)	FEA cracked GFRP mode (m, n)
1			7		
2			8		
3			9		
4			10		
5			11		
6			12		



Fig. 9. Experimental modal analysis of cracked GFRP pipes.

The results of the experimental modal analysis including natural frequency and damping ratio are presented in Tables 4 and 5 for healthy and cracked GFRP respectively.

Table 4
Experimental natural frequencies and damping ratios for healthy GFRP.

Mode (m, n)	Natural frequencies (Hz)	Damping ratio (%)
1 (1,2)	1825	0.57
2 (1,2)	1825	0.57
3 (1,2)	1862	0.13
4 (1,2)	1862	0.13
5 (2,2)	2201	0.62
6 (2,2)	2201	0.62
7 (1,0)	2908	0.72
8 (1,0)	2908	0.72

Furthermore, the comparison between the obtained natural frequencies with the following three methods of theoretical analysis, finite element method and experimental modal analysis are presented in Tables 6 and 7:

Table 6
Comparison of the natural frequencies (Hz) of healthy GFRP under Free-Free boundary condition.

Mode (m, n)	Healthy reinforced steel tube with glass fiber composites			Comparison the percentage of errors of different methods together		
	Analytic	FEA	EMA	Analytic-FEA (%)	Analytic-EMA (%)	FEA-EMA (%)
1 (1,2)	1810.42	1812.2	1825	0.09	0.80	0.70
2 (1,2)	1810.42	1812.2	1825	0.09	0.80	0.70
3 (1,2)	1842.34	1848.9	1862	0.35	1.06	0.71
4 (1,2)	1842.34	1848.9	1862	0.35	1.06	0.71
5 (2,2)	2145.41	2120.8	2201	0.16	2.60	2.43
6 (2,2)	2145.41	2120.8	2201	0.16	2.60	2.43
7 (1,0)	2782.36	2263.4	2908	0.54	4.51	3.95
8 (1,0)	2782.36	2263.4	2908	0.54	4.51	3.95

Table 8 shows the difference between first four natural frequencies of healthy and cracked specimen GFRP pipe quantitatively based on experimental modal analysis. According to the results of the natural frequencies shown in Tables 6, 7 and 8, the following results have been were obtained.

Table 5
Experimental natural frequencies and damping ratios for cracked GFRP.

Mode (m, n)	Natural frequencies (Hz)	Damping ratio (%)
1 (1,1)	1751.33	0.56
2 (1,2)	1780.31	0.12
3 (1,2)	1795.62	0.52
4 (1,2)	1900.43	0.47
5 (1,2)	2095.20	0.61

According to Table 6, it is observed that some of the natural frequencies obtained for a healthy GFRP are repeated which is because of the axial symmetry of GFRP pipe and geometrical symmetry. However, according to Table 7, the reason for this is the presence of cracks in the pipe, which causes the body to move out of the axial symmetry state. By comparing Tables 6 and 7 together, it is concluded that the presence of crack in the desired pipe reduces the natural frequencies, which affects the decrease of stiffness of cracked pipe. Also, one can see that the repeated natural frequency for the cracked pipe does not exist. This is because of the presence of crack. By comparing the three theoretical analysis methods, finite element simulation and experimental modal analysis, it follows that the percentage error of calculation in the results of these three methods is low and this indicates the high accuracy in the calculations and measurements. The graphs of the frequency response functions related to a healthy and cracked GFRP are expressed in Figs. 10 and 11.

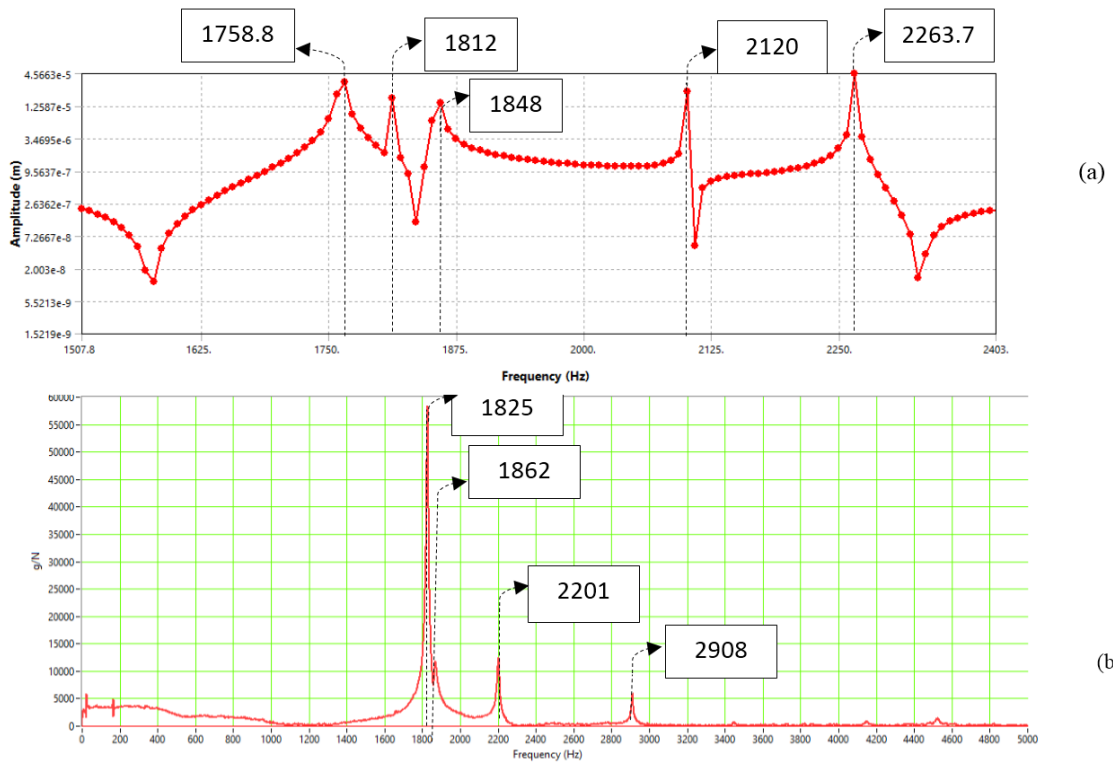


Fig. 10. Frequency response function diagram of healthy GFRP pipe obtained by a) Finite element simulation method, b) Experimental modal analysis method for the first and second natural frequencies.

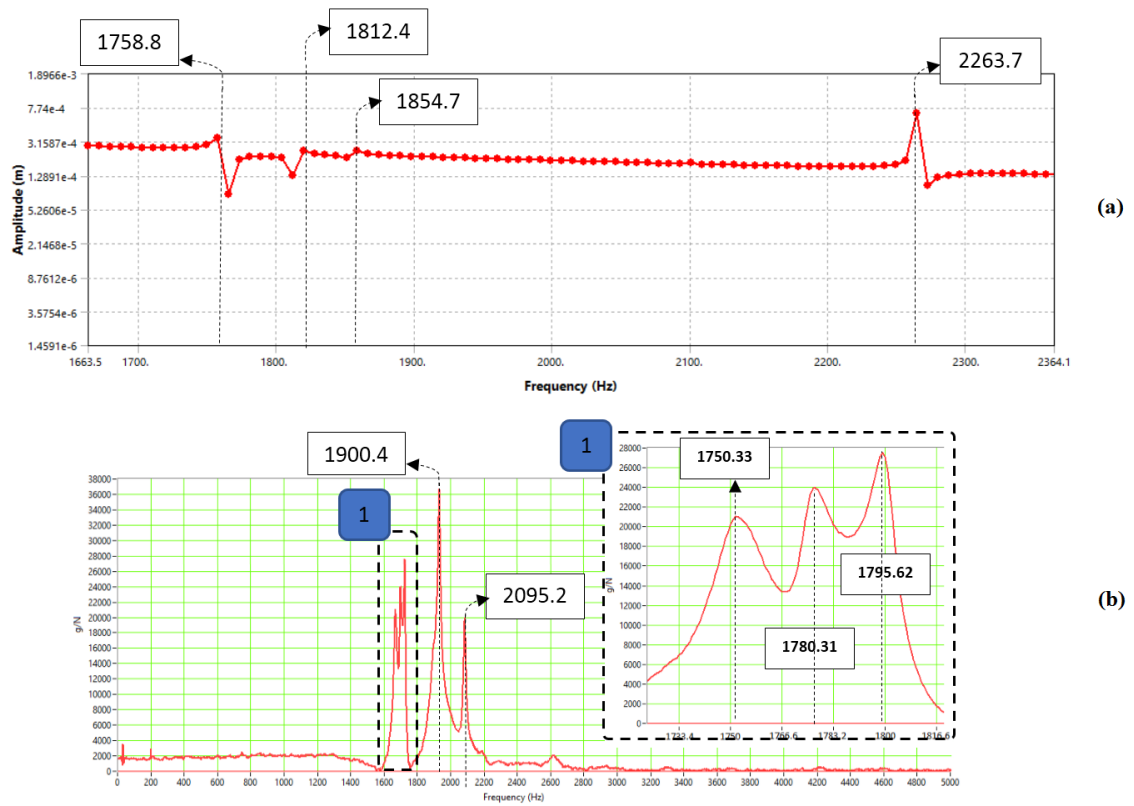


Fig. 11. Frequency response function diagram of cracked GFRP pipe obtained by a) Finite element simulation method, b) Experimental modal analysis method.

Table 7
Comparison of the natural frequencies (Hz) of cracked GFRP under Free-Free boundary condition.

Cracked reinforced steel tube with glass fiber composites			
Mode (<i>m, n</i>)	FEA	EMA	Error (%)
1 (1,1)	1758.8	1751.33	0.42
2 (1,2)	1811	1780.31	1.72
3 (1,2)	1812.4	1795.62	0.93
4 (1,2)	1848	1900.43	2.83
5 (1,2)	1854.7	2095.20	12.96

Table 8
Difference between natural frequencies of healthy and cracked reinforced steel tube with glass fiber composites pipes.

Mode	EMA (healthy)	EMA (cracked)	Difference (Hz)
1	1825	1751.33	74
2	1862	1780.31	81.69
3	2201	1900.43	301
4	2908	2095.2	812.8

6. Conclusions

The purpose of this study was to obtain modal parameters (natural frequencies, shape of mods and frequency response diagrams) for a GFRP reinforced steel pipe in two healthy and cracked conditions. The results were analyzed in three ways: theoretical analysis, FEM and experimental modal analysis were performed and the results are presented in the fourth chapter of the study.

One of the topics discussed in this study was that the different layers of composite fibers reinforcing the desired steel pipe which would have an effect on the results. The results of this study showed that the carbon/epoxy composite fibers are more resistant to glass/epoxy than hardware, and this has a direct impact on the modal parameters of the object. This effect is that no matter how hard the object is, the natural frequencies increase and this is observed in the results. But, the reason for the use of glass/epoxy composite fibers was that the fiber is more cost-effective in terms of manufacturing cost compared to other composite fibers, such as carbon/epoxy, and access to this type of fiber is easier. Another important issue mentioned in this study is the cracks' discussion and its various modes and their impact on the modal parameters of the tube. According to the obtained results, the presence of cracks on each piece decreases the hardness, and consequently the corresponding natural frequencies decrease. According to the material in the failure mechanics, in the definition of the crack, only the geometric shape can be resembled is an ellipse whose small diameter tends to zero. The maximum length of the crack should be $\frac{1}{4}$ of the circumference of the object. By examining different types of cracks (in terms

of dimensions, angles, and placement coordinates), the results showed that the three-dimensional cracking had the greatest effect on the modal parameters of the pipe.

References

- [1] J.Q. Ye, Laminated Composite Plates and Shells: 3D Modeling, Springer-Verlag London Publisher, (2003).
- [2] A. Bhimaraddi, Free vibration analysis of doubly curved shallow shells on rectangular planform using three dimensional elasticity theory, *Int. J. Solids Struct.*, 27(7) (1991) 897-913.
- [3] W.J. Wang, K. Lin, Free vibration of laminated plates using a finite strip method based on a higher-order plate theory, *Comput. Struct.*, 53(6) (1994) 1281-1289.
- [4] J. Xiaoyu, 3-D vibration analysis of fiber reinforced composite laminated cylindrical shells, *J. Vib. Acoust.*, 119(1) (1997) 46-51.
- [5] Y.M. Tsai, Longitudinal motion of a thick transversely isotropic hollow cylinder, *J. Pressure Vessel Tech.*, 113(4) (1991) 585-589.
- [6] K. Xu, A.K. Noor, W.S. Burton, 3D solutions for free vibration of initially stressed thermoelectroelastic multilayered cylinders, *J. Eng. Mech.*, 123(1) (1997) 45-51.
- [7] J.Q. Ye, K.P. Soldatos, Three-dimensional vibration of laminated composite plates and cylindrical panels with arbitrarily located lateral surfaces point supports, *Int. J. Mech. Sci.*, 38(3) (1996) 271-281.
- [8] J.Q. Ye, K.P. Soldatos, Three-dimensional vibrations of cross-ply laminated hollow cylinders with clamped edge boundaries, *J. Vib. Acoust.*, 119(3) (1997) 317-323.
- [9] K. Ding, L. Tang, Three-dimensional free vibration of thick laminated cylindrical shells with clamped edges, *J. Sound Vib.*, 220(1) (1999) 171-177.
- [10] C.Q. Chen, Y.P. Shen, Three-dimensional analysis for the free vibration of finite-length orthotropic piezoelectric circular cylindrical shells, *J. Vib. Acoust.*, 120(1) (1998) 194-198.
- [11] W.Q. Chen, J. Ying, Q.D. Yang, Free vibrations of transversely isotropic cylinders and cylindrical shells, *J. Pressure Vessel Tech.*, 120(4) (1998) 321-324.

- [12] Y.C. Chern, C.C. Chao, Comparison of natural frequencies of laminates by 3-D theory, Part II: curved panels, *J. Sound Vib.*, 230(5) (2000) 1009-1030.
- [13] A.E.H. Love, *A Treatise on the Mathematical Theory of Elasticity*, 1st edition (Cambridge University Press, Cambridge) 4th edition., Dover Publishing, New York, (1944).
- [14] M.S. Qatu, On the validity of nonlinear shear deformation theories for laminated composite plates and shells, *Compos. Struct.*, 27(4) (1994) 395-401.
- [15] W.T. Koiter, *Theory of Thin Shells*, ed. F.L. Niordson, Springer-Verlag Publisher, New York, (1969) 93-105.
- [16] A.L. Gol'denveizer, *Theory of Elastic Thin Shells English Translation*, Pergamon Press, New York, (1961).
- [17] A.K. Noor, W.S. Burton, Assessment of computational models for multilayered composite shells, *Appl. Mech. Rev.*, 43(4) (1990) 67-97.
- [18] P.M. Naghdi, J.G. Berry, On the equations of motion of cylindrical shells, *J. Appl. Mech.*, 21 (1964) 160-166.
- [19] J.H.S. Almeida, M.L. Ribeiro, V. Tita, S.C. Amico, Damage and failure in carbon epoxy filament wound composite tubes under external pressure: experimental and numerical approaches, *Mater. Des.*, 96 (2016) 431-438.
- [20] T. Üstün, V. Eskizeybek, A. Avci, Enhanced fatigue performances of hybrid nanoreinforced filament wound carbon/epoxy composite pipes, *Compos. Struct.*, 150 (2016) 124-131.
- [21] M.L. Ribeiro, D. Vandepitte, V. Tita, Experimental analysis of transverse impact loading on composite cylinders, *Compos. Struct.*, 133 (2015) 547-563.
- [22] H. Zhou, Z. Pan, R.K. Gideon, B. Gu, B. Sun, Experimental and numerical investigation of the transverse impact damage and deformation of 3-D circular braided composite tubes from meso-structure approach, *Compos. Part B: Eng.*, 86 (2016) 243-253.
- [23] H. Luo, Y. Yan, X. Men, C. Jin, Progressive failure analysis and energy-absorbing experiment of composite tubes under axial dynamic impact, *Compos. Part B: Eng.*, 87 (2016) 1-11.
- [24] V.S. Sokolinsky, K.C. Indermuehle, J.A. Hurtado, Numerical simulation of the crushing process of a corrugated composite plate, Part A: *Compos. Appl. Sci. Manuf.*, 42(9) (2011) 1119-1126.
- [25] M. Hemmatnezhad, G.H. Rahimi, M. Tajik, F. Pellicano, Experimental, numerical and analytical investigation of free vibrational behavior of GFRP-stiffened composite cylindrical shells, *Compos. Struct.*, 120 (2015) 509-518.
- [26] J.S. Yang, J. Xiong, L. Ma, L.N. Feng, S.Y. Wang, L.Z. Wu, Modal response of all-composite corrugated sandwich cylindrical shells, *Compos. Sci. Technol.*, 115 (2015) 9-20.
- [27] S. Gurgun, M.A. Sofuglu, Experimental investigation on vibration characteristics of shear thickening fluid filled CFRP tubes, *Compos. Struct.*, 226 (2019) 111-236.
- [28] A. Capozucca, E. Magagnini, Experimental vibration response of homogeneous beam models damaged by notches and strengthened by CFRP lamina, *Compos. Struct.*, 206 (2018) 563-577.
- [29] M. Sit, C., Ray, Free vibration characteristics of glass and bamboo epoxy laminates under hygrothermal effect: A comparative approach, *Compos. Part B: Eng.*, 176 (2019) 107333.
- [30] Z. Yu, L. Zhang, J. Hu, Cracked modeling and vibration analysis of pipe with a part-through crack, *J. Vibro Eng.*, 19(2) (2017) 930-942.
- [31] Egyptian code of practice for steel construction and bridges (Allowable stress design- ASD): Code No. 279, Housing and building national research center, Ministry of Housing, Utilities and Urban Development and Permanent Committee for the Code of Practice for Steel Construction and Bridges, Arab Republic of Egypt, (2001).
- [32] M. Gopalakrishnan, S. Muthu, R. Subramanian, R. Santhanakrishnan, L.M. Karthigeyan, Tensile properties study of E-Glass/Epoxy laminate and $\pi/4$ quasi- isotropic E-Glass/Epoxy laminate., *Polym. Polym. Compos.*, 24(6) (2016) 429-446.
- [33] I. Ortiz de Mendibil, L. Aretxabaleta, M. Sarriollandia, M. Mateos, J. Aurrekoetxea, Impact behaviour of glass fibre-reinforced epoxy/aluminium fibre metal laminate manufactured by Vacuum Assisted Resin Transfer Moulding, *Compos. Struct.*, 140 (2016) 118-124.
- [34] R. Allemang, *Analytical and Experimental Modal Analysis*, Department of Mechanical, PhD Thesis, Industrial and Nuclear Engineering University of Cincinnati, Ohio., 219 (1999).
- [35] S. Rad, *Introduction to Modal Analysis*, Department of Mechanical Engineering, Isfahan University of Technology, Iran, (2012).

- [36] C. Tao, Y. Fu, T. Dai, Dynamic analysis for cracked fiber-metal laminated beams carrying moving loads and its application for wavelet based crack detection, *Compos. Struct.*, 159 (2017) 463-470.
- [37] A.V. Lopatin, E.V. Morozov, Fundamental frequency of the laminated composite cylindrical shell with clamped edges, *Int. J. Mech. Sci.*, 92 (2015) 35-43.
- [38] H. Allahbakhsh, M. Shariati, Instability of cracked CFRP composite cylindrical shells under combined loading, *Thin-Walled Struct.*, 74 (2014) 28-35.